Biogeosciences Discuss., 9, 16625–16662, 2012
www.biogeosciences-discuss.net/9/16625/2012/
doi:10.5194/bgd-9-16625-2012

Biogeosciences Discussions

NW European shelf under climate warming: implications for open ocean – shelf exchange, primary production, and carbon absorption

M. Gröger[1], **E. Maier-Reimer**[1], **U. Mikolajewicz**[1], **A. Moll**[2], **and D. Sein**[1]

[1]Max Planck Institute for Meteorology, Bundesstrasse 53, 20146 Hamburg, Germany
[2]Institut für Meereskunde, Universität Hamburg, Bundesstrasse 53, 20146 Hamburg, Germany

Received: 7 November 2012 – Accepted: 9 November 2012 – Published: 21 November 2012

Correspondence to: M. Gröger (matthias.groeger@zmaw.de)

Published by Copernicus Publications on behalf of the European Geosciences Union.

Abstract

Shelves have been estimated to account for more than one fifth of the global marine primary production. It has been also conjectured that shelves strongly influence the oceanic absorption of atmospheric CO_2 (carbon shelf pump). Owing to their coarse resolution, currently applied global climate models are inappropriate to investigate the impact of climate change on shelfs and regional models do not account for the complex interaction with the adjacent open ocean. In this study, a global ocean general circulation model and biogeochemistry model were set up with a distorted grid providing a maximal resolution for the NW European shelf and the adjacent North Atlantic.

Using model climate projections we found that already a moderate warming of about 2.0 K of the sea surface is linked with a reduction by ~30 % of biological production on the NW European shelf. If we consider the decline of anthropogenic riverine eutrophication since the 90's the reduction of biological production amounts to 39 %. The decline of NW European shelf productivity is twice as strong as the decline in the open ocean (~15 %). The underlying mechanism is a spatially well confined stratification feedback along the continental shelf break. This feedback reduces the nutrient supply from the deep Atlantic to about 50 %. In turn, the reduced productivity draws down CO_2 absorption on the NW European shelf by ~34 % at the end of the 21st century compared to the end of the 20th century implying a strong weakening of shelf carbon pumping. Sensitivity experiments with diagnostic tracers indicate that not more than 20 % of the carbon absorbed in the North Sea contributes to the long term carbon uptake of the world ocean. The rest remains within the ocean mixed layer where it is exposed to the atmosphere.

The predicted decline in biological productivity and decrease of phytoplankton concentration (by averaged 25 %) due to reduced nutrient imports from the deeper Atlantic will probably negatively affect the local fish stock and therefore fisheries in the North Sea.

BGD

9, 16625–16662, 2012

1 Introduction

Because of their high biological productivity shelves have been proposed to play a major role in the absorption of atmospheric CO_2 by fixing dissolved inorganic carbon (DIC) into organic soft tissue which lowers sea water pCO_2 and draws CO_2 from the atmosphere into the water. Therefore, most mid and high latitude shelves have been recognized to be significant sinks for atmospheric CO_2 (e.g. Chen and Borges, 2009). As part of the carbon is exported to the open ocean, Tsunogai et al. (1999) proposed the term "continental shelf pump" to describe an additional carbon pump mechanism besides the carbonate and the soft tissue pumps (Raven and Falkowski, 1999). From local case studies in the East China Sea and the North Sea it has been estimated that the shelf pump may account for 30 % to 50 % of the global ocean's net annual carbon uptake (Tsunogai et al., 1999; Thomas et al., 2004). The North Sea which constitutes a significant area within the NW European shelf has likewise been intensely monitored during the last decades and was found to act as a significant sink for atmospheric carbon (e.g. Thomas et al., 2004).

Besides its role in the carbon cycle, continental shelves are also important for economic fisheries as they support over 90 % of global fish catches (Pauly et al., 2002). There is much evidence that some fish populations and fish recruitment are highly vulnerable to climate due to changing water temperature and planktonic ecosystems (Beaugrand, 2004).

Biological production depends on the availability of nutrients which are supplied to the shelf by upwelling and lateral advection from the deep ocean, and by continental runoff. The nutrient supply from the deep ocean is controlled by the topography along the shelf break which is marked by abrupt depth changes, steep ridges and deep channels. Here, generation of internal waves and turbulent eddies induce intense upward mixing of dissolved nutrients. In addition, turbulence is produced by breaking tidal waves (New and Pingree, 1990). Such processes are characteristic for the NW European shelf (e.g. Pingree and Mardell, 1981; Joint et al., 2001; Green et. al., 2008; Bergeron and Koueta, 2011) and thus, determine the nutrient supply to the shelf. However, these important processes along shelf break are not sufficiently represented neither in global ocean models where the narrow shelf break is not resolved, nor in regional shelf models where cross shelf break exchange has to be prescribed (e.g. Lorkowski et al., 2012). Moreover, most global models used in climate studies do not treat tides at all.

In this paper we address the future evolution of nutrient transport from the Atlantic into the North Sea and subsequent changes in biological productivity in response to the anthropogenic climate change as predicted for the 21st century. To overcome the aforementioned specific problems associated with both, regional and global models, in this study a global ocean general circulation model (OGCM) with gradually increased resolution on the NW European shelf coupled to a marine carbon cycle and biogeochemical carbon cycle model is established and applied for future climate projections.

2 Model description

2.1 The physical global ocean circulation model

The physical model is the Max-Planck-Institute for Meteorology global primitive equation OGCM (MPIOM). It is a z-level model with a free surface. The model assumes the hydrostatic and Boussinesq approximations. It includes a dynamic thermodynamic sea ice model following Hibler (1979). Tracer and momentum advection follows a second order total variation diminishing scheme after (Sweby, 1984). The model's equations are discretized on a bipolar orthogonal curvilinear C-grid. The water column is subdivided by 30 layers eight of which lie within the uppermost 100 m. A detailed model description and validation of physical properties is given in Marsland et al. (2003).

The model's grid has been set up with a resolution of nominal 1.5° and the grid poles are placed over Central Europe (49° N, 8° E) and North America (44° N, 89° W) in order to maximize the resolution for the NW European shelf (10 km in the North Sea) and for

BGD
9, 16625–16662, 2012

the adjacent North Atlantic. Figure 1 shows the model domain of the applied grid setup focusing on the NW European shelf/North Atlantic. As the tidal movement is important both, for vertical mixing, and for the transport by the residual currents on continental shelves, the full potential of lunisolar tidal forces is prescribed according to Thomas et al. (2001). The appropriate simulation of tides requires a relatively short time step of 45 min. A detailed and comprehensive description of the physical setup will be given in Sein et al. (2012).

2.2 The carbon cycle and biogeochemistry model

Embedded in the physical model is the biogeochemical module HAMOCC (HAMburg Ocean Carbon Cycle model, Wetzel et al., 2005), i.e. it uses the same grid configuration as MPIOM and the advection and diffusion of biogeochemical tracers are identical to temperature and salinity.

HAMOCC is a modified Nutrient, Phytoplankton, Zooplankton, Detritus (NPZD-type) biogeochemistry model. In case of sufficient light, phytoplankton growth is limited by dissolved phosphate (PO_4), nitrate (NO_3), and iron which are fixed into organic soft tissue together with DIC following Redfield stoichiometry during photosynthesis. The detritus pool is formed by dead phyto- and zooplankton and fecal pellets. Besides these biomass groups dissolved organic matter is formed from excretion of living biomass. All organic matter is remineralized to inorganic constitutents by consumption of oxygen or alternatively, by reduction of nitrate (denitrification) or eventually sulphate. At the sea floor the model is closed by a 12 layer sediment model following Heinze et al. (1999). Air-sea gas exchange is calculated from the local pCO_2 difference according to Wanninkhof (1992) with an improved temperature dependency (Gröger and Mikolajewicz, 2011). A detailed technical model description is provided by Maier-Reimer et al. (2005).

We also implemented global riverine inputs of PO_4, NO_3, DIC, Fe, Si in the model. Mean values for riverine inputs were prescribed based on the estimates from a global dataset (Meybeck and Ragu, 1995). With this configuration the coupled ocean-biogeochemistry model provides a resolution in the area of interest which is

BGD
9, 16625–16662, 2012

comparable with many regional models (e.g. Moll and Raddach, 2003). Since it is a global model, however, it avoids the uncertainties due to the prescription of energy and mass fluxes at the bounds of regional models.

In order to improve the models performance in simulating the seasonal cycle of nutrients and phytoplankton we had to modify the light penetration scheme of the biogeochemistry odel HAMOCC. Details of this light penetration scheme are given in the appendix.

3 Experiments

The model was spun up for several thousand years by forcing the model repeatedly with 6-hourly atmospheric fields taken from the ECHAM5/MPIOM IPCC AR 4 preindustrial control run (Roeckner et al., 2006).

The experiments listed in Table 1 are designed to investigate the effects of climate warming, rising atmospheric $p\mathrm{CO_2}$, and anthropogenic eutrophication separately. For this, experiments CWE, CWE-CEE, and CWE-CEE-AES were started and forced by the atmospheric output from the MPI-ECHAM5 IPCC AR 4 20th century and A1B scenario simulations between 1860 and 2100. In experiment CWE the pure effect of climate warming was tested by keeping the atmospheric $p\mathrm{CO_2}$ fixed at the 288 ppm for the biogeochemistry model. Experiment CWE-CEE includes also the rise of atmospheric $p\mathrm{CO_2}$ for the biogeochemistry model and run CWE-CEE-AES includes both, rising atmospheric $p\mathrm{CO_2}$ and an anthropogenic eutrophication scenario for the NW European shelf which today receives riverine nutrients from industrial agriculture. Thus, river concentrations of dissolved phosphorous and nitrate were exponentially increased from 1860 onward to match observations available between 1976 and 2006 (updated data from Paetsch and Lenhart, 2004). After 2006 monthly mean values from the last 5 yr were repeated to 2100. Thus, there is no trend in riverine nutrient supply during the 21st century. Run CTRL continues the spinup-simulation which allows to separate between real signals and residual model drift.

In addition, two sensitivity experiments were conducted to investigate the efficiency of the carbon shelf pump exemplary for North Sea and the adjacent Atlantic (Table 1). In run CO_2-NS atmospheric pCO_2 was locally set to 1112 ppm over the North Sea only to study the effect on the global carbon cycle. Experiment MARKER was carried out to study the fate of North Sea water after it leaves the North Sea, i.e. does it really reach the deep ocean or does it remain within the ocean's mixed layer where it is exposed to the atmosphere and subject to air sea gas exchange.

4 Model performance and validation

As a prerequisite to applying the IPCC A1B climate projections the performance of the global and regional model must be examined in order to determine the extent to which the control period reproduces past climate/ecosystem (hindcast) conditions. In the following section we validate the results of experiment CWE-CEE-AES as it includes both, the effects of rising atmospheric pCO_2 and the anthropogenic eutrophication in the North Sea. Thus, this set up is closest to reality. We concentrate primarily on the modelled distributions of dissolved nutrients since these variables integrate the different processes related to advection, diffusion, biological consumption and production, decomposition, remineralization, and temperature.

In the first part of the following section we compare the modelled global distributions with observation based estimates from the World Ocean Atlas (WOA, Garcia et al., 2010). In the second part we test the model performance particularly in the North Sea by visual and quantitative comparison to observations.

4.1 Global ocean

In general, the modeled surface phosphate concentration compares well with observed patterns (Fig. 2). Highest concentrations are located in the northernmost Pacific where nutrient rich abyssal waters rise, and in the high latitude southern ocean where deep

BGD
9, 16625–16662, 2012

convection around Antarctica maintains nutrient supply from deeper layers. Enhanced concentrations are also associated with the wind driven Eastern Pacific equatorial divergence, and the upwelling along the coasts of Western Africa and Western South America. The Northern North Atlantic is marked by a pronounced seasonal cycle which is mainly caused by the nutrient consuming biological productivity during spring and summer and nutrient accumulation during winter. Lowest concentrations are seen in the subtropical gyres which are marked by downward Ekman pumping and a thin mixed layer.

The vertical nutrient distributions are shown in Fig. 3. The main deep and intermediate waters can be well recognized by their nutrient content. Along the Atlantic section nutrient poor North Atlantic Deep Water (NADW) causes low nutrient concentrations between 1800 and 4000 m water depths. In the Southern ocean at deeper layers the nutrient content is slightly underestimated compared to observations due to the somewhat too weak production of Antarctic Bottom in the model. Pronounced features of the Atlantic section are the nutrient rich Antarctic Intermediate water which gains nutrients by remineralization of organic matter, and the North Atlantic where nutrient depleted surface waters are transfered to depth due to deep convection. Due to the conveyor belt circulation the Pacific Ocean is generally nutrient richer compared to the Atlantic. The highest nutrient concentrations are reached in the North Pacific at intermediate depths between 1000 and 2000 m. This is somewhat underestimated by the model. In both, the Atlantic and Pacific Ocean, Ekman pumping in the subtropical gyres transfers nutrient depleted surface waters to depths. In the Pacific, the Southern Hemisphere subtropical convergence cell extents deeper than the one in the Northern Hemisphere which compares well with observations from the WOA. Well represented is as well the nutrient poor North Atlantic where deep water formation. Globally integrated fluxes of CO_2, primary production, and export production are well within the range of published values (Table 2).

BGD
9, 16625–16662, 2012

4.2 North Sea

For a realistic simulation of biogeochemical cycles it is essential to model a realistic flow pattern not only for the North Sea but for the adjacent open Atlantic as well. Atlantic waters enter the North Sea mainly at its northern boundary through the straits of Fair Isle and Pentland Firth and through the English Channel in the west (Fig. 1). Waters leave the North Sea along the Norwegian trench and are further transported towards the Arctic via Norwegian Current. The modeled water mass net exchange along the northern boundary and through the English Channel compares well with observations based estimation of Thomas et al. (2005, Table 2). Likewise, the net mass transports of carbon across the boundaries are in good agreement with observations. With the exception of the net carbon export across the northern boundary, differences between the modeled transports and the observations are clearly smaller than the models standard deviation. The modelled absorption of atmospheric carbon amounts to $0.9\,\mathrm{Tmol\,yr^{-1}}$. This corresponds to a mean absorption of $1.5\,\mathrm{mol\,C\,m^{-2}}$ which is close to the estimate of $1.3\,\mathrm{mol\,C\,m^{-2}}$ given by Lorkowski et al. (2012) and the observation based estimate of Thomas et al. (2005) ($1.4\,\mathrm{mol\,C\,m^{-2}}$).

The models annually integrated primary production amounts to $6.5\,\mathrm{mol\,C\,m^{-2}}$. This is clearly lower compared to other models which range between 12 and 18 $\mathrm{mol\,m^{-2}}$ (Moll, 1998; Moll and Raddach, 2003; Kühn et al., 2010; Lorkowski et al., 2012). The lower biological production is in part related to the fact that we did not include the atmospheric nitrogen deposition in our simulations (Paetsch and Kühn, 2008). Including the atmospheric nitrogen input would have enhanced the productivity strongly on the outer shelf which in our model is limited by nitrate whereas near the coast it is limited by phosphorous.

Figure 4 shows a north-south transect of dissolved phosphate profiles through the North Sea comparing observed and simulated profiles for May, averaged from 1993–2008 (Grosse and Moll, 2011). The model reproduces the stratification in spring and thus matches the observed profile of phosphate concentration in many of the boxes.

Box 15 and 23 in the Northern North Sea illustrate the feature of a deep reaching nutricline, as a transition from depleted nutrients at the surface at 10 m depth to homogeneous concentrations at 50 m depth down to the bottom. Stratification in the Central North Sea (boxes 34 and 47) is different and characterized by a well-mixed surface zone (0–30 m), a short transition with a jumped increase in concentration over 10–20 m, and homogeneous concentrations at depth. The model tends to overestimate the surface concentration. The Southern North Sea is characterized by well-mixed profiles. The simulated concentrations are sometimes over- or underestimated compared to observations. The simulated variability, however, is in magnitude for many boxes comparable to observations.

The results of the quantitative validation are summarized in Table 3. The model is able to represent the physical variables of the North Sea, either in terms of the bulk property (root mean square difference) and variability (correlation, and standard deviation). For the comparison of nutrients, phosphate and nitrate are quantified. The correlation for nutrients is lower (0.58/0.43) compared to temperature and salinity. The simulated and observed standard deviations match best for salinity.

5 Stratification on the shelf and along the shelf break

The NW European shelf warms between 1.6 K in off shore areas and 3.2 K near the coasts in response to the IPCC AR4 A1B warming scenario. In the North Sea the annually averaged surface temperature increases by nearly 2 K in the course of the 21st century (Fig. 5a). This is somewhat lower than the model's global average warming of 2.5 K. The atmospheric forcing is also marked by an intensifying hydrological cycle which leads to enhanced moisture transports from the tropics to high latitudes. North of 40° N the Atlantic freshens considerably. The North Sea as a shelf basin which is widely surrounded by land is also strongly affected by continental runoff. The enhanced river runoff results in a considerably stronger freshening in comparison with the open Atlantic and the sea surface salinity decreases by 0.75 psu (Fig. 5a) at the end of the

BGD
9, 16625–16662, 2012

21st Century. The freshening of the bottom layer is weaker than at the surface since the North Sea still receives saltier waters from the adjacent North Atlantic. Accordingly, the bottom to surface salinity difference increases by 0.1 psu (or 25 %) (Fig. 5b) in the course of the 21st century. The shelf, thus, undergoes considerably enhanced stratification.

The stratification is accompanied by a strong decline of nutrient transports from the Atlantic into the North Sea during the second half of the 21st century. The nutrient supply take places mainly during winter when vertical mixing is strongest throughout the year and nutrients are not consumed by biological activity due to limitation of biological production by light. In all climate change experiments the transport of dissolved phosphate and nitrate at the northern boundary of the North Sea is nearly halved (Fig. 5g, h) compared to preindustrial levels.

The decline in winter nutrient supply in the second half of the 21st century (Fig. 5g, h) is not caused by a weaker inflow of Atlantic water masses northeast off Scotland. Instead, Atlantic water masses entering the North Sea have lower nutrient concentrations compared to the 20th Century. This nutrient depletion is caused by weaker vertical mixing along the shelf break and the continental slope which, in turn, is caused by hydrographic changes. Over the shelf break and the continental slope, the upper 100 m of the Atlantic have warmed by 1 K and freshened by 0.25 psu at the end of the 21st century, whereas at intermediate depths only very small changes of temperature and salinity are predicted (Fig. 5c, d). As a result of this enhanced stability of the water column, the shelf break mixing weakens and, accordingly, the winter mixed layer depth shallows by up to several hundred meters along the shelf break (Fig. 6a, b). Accordingly, the upward mixing of nutrient rich waters from below the photic zone to shallower water depths is essentially reduced. Wide areas of the NW European shelf have been virtually cut off from the mid-depth Atlantic nutrient source. As a result, nutrient supply from the Atlantic to the shelf breaks down and the nutrient inventory on the shelf diminishes. In the Northern North Sea the nutrient concentrations are lowered locally by up to 50 % compared to the end of the 20th century (Fig. 6c, d). The Southern North Sea is less affected as the nutrient rich water masses from the north usually divert eastward when they reach the Central North Sea.

5.1 Decline in biological productivity

Due to the reduced winter nutrient import from the Atlantic, the nutrient inventory of the North Sea diminishes by 33 % at the end of the 21st century in the experiments without anthropogenic eutrophication CWE and CWE-CEE. This results in lower biological production in the North Sea which reduces by ~31 % in experiments CWE and CWE-CEE from the last two decades of the 20th century to end of the 21st century (Fig. 5e, Table 4). The reduction of North Sea productivity is of similar magnitude as for the entire NW European shelf where the reduction varies between 30 % and 39 % in the respective experiments (Table 4). Remarkably, the productivity decline on the shelf is much stronger than in the open ocean. For the open North Atlantic and the global ocean our model predicts a productivity reduction of only 17 % and 15 % respectively which agrees well with results from other models which predict reductions between 2 % and 20 % resulting from higher open ocean stratification (Steinacher et al., 2010). We thus conclude that the NW European shelf productivity is much more vulnerable to climate warming than the open ocean. The higher vulnerability arises from the above described stratification feedback along the shelf break. This feedback acts in addition to the well-known stratification impact on marine productivity in the open ocean.

In experiment CWE-CEE-AES the evolution of production is strongly modified by the prescribed anthropogenic eutrophication. In the course of the 20th century the riverine nutrient discharges from industrial agriculture and detergents strongly increased (Paetsch and Lenhart, 2004) and stimulated productivity. Between 1975 and 1985, when prescribed discharges were highest, biological production in the North Sea is enhanced by 38.5 % compared to the simulations CWE-CEE and CWE without this effect (Fig. 5e). The anthropogenically enhanced productivity is mainly restricted to the coastal regions of the Southern and Southeastern North Sea. In the early 1990's, the prescribed anthropogenic riverine nutrient input strongly declined which explains the

BGD
9, 16625–16662, 2012

large drop in productivity at the end of the 20th century in experiment CWE-CEE-AES. In this experiment the stratification feedback along the shelf edge leads to a decline of North Sea productivity in the course of the 21st century as well (Fig. 5e). Here, uncertainties are associated with the chosen scenario for 21st century nutrient discharges.

5.2 Impact of rising pCO_2 and declining productivity on carbon absorption

Consistent with many studies based on observations (e.g. Frankignoulle and Borges, 2001; Thomas et al., 2005) our simulations show that the North Sea is a sink for atmospheric CO_2. The yearly integrated carbon absorption varies between 9.3 and 11.8 Mt C for the last two decades of the 20th century (Table 4) in agreement with published values based on observations (9.5 Mt C, Thomas et al., 2005). Interestingly, the rising atmospheric pCO_2 in experiment CWE-CEE has nearly no effect on carbon absorption in the North Sea (Fig. 5f, blue line). In this experiment carbon absorption is hardly higher than in experiment CWE without rising atmospheric pCO_2. As the air-sea exchange for CO_2 can be characterized – including the buffering of the carbonate system – by a piston velocity of 100 m yr^{-1}, the North Sea is almost in equilibrium with rising atmospheric levels of CO_2. In experiment CWE-CEE carbon absorption in the last two decades of the 20th century is only by 0.59 Mt higher (= 6.3 %) than in experiment CWE (Table 4) although the atmospheric pCO_2 has risen by 22 %. At the end of the integrations carbon absorption in experiment CWE is even higher than in CWE-CEE although the atmospheric pCO_2 was kept fix at the preindustrial level in run CWE. In all experiments, the Atlantic water masses entering the North Sea decrease in DIC because the rising water temperatures lower the solubility of CO_2 and enhanced stratification reduces the upward mixing of DIC rich water masses from the deep Atlantic. This lowers the DIC imports from the Atlantic which, in turn, will lower the local water pCO_2 in the North Sea and thus enhance carbon absorption. In experiments CWE-CEE and CWE-CEE-AES, however, the DIC decrease in the adjacent Atlantic is not significant as the upper ocean pCO_2 adapts rapidly to the rising atmospheric pCO_2.

BGD
9, 16625–16662, 2012

Changes in biological productivity have a stronger impact on carbon absorption of the North Sea than the rising atmospheric pCO_2. Thus, in experiment CWE-CEE-AES absorption is enhanced by about 25 % between 1975 and 1985 compared to run CWE-CEE Fig. 5f). In all experiments the decreasing biological productivity in the course of the 21st century strongly reduces atmospheric carbon absorption (Fig. 5f). The relative reductions in carbon absorption range between 23 % and 37 % for the North Sea and 12 % and 32 % for the entire NW European shelf (Table 4). The strongest decline is simulated in experiment CWE-CEE-AES (37 % in the North Sea) which likewise exhibits the strongest decline in productivity. Part of this decrease is a direct consequence of the assumed reduction in anthropogenic eutrophication. However, in the experiment CWE-CEE without anthropogenic nutrient input, the net uptake of anthropogenic CO_2 is still reduced by 34 %.

6 Does continental shelf pumping really enhance the oceanic storage of carbon?

Strong absorption on the shelf does not necessarily result in long term oceanic carbon sequestration since a large portion of the shelf water exported to the open ocean remains within the mixed layer and does not reach the deep ocean. In the following we describe two experiments that were designed to estimate how much anthropogenic carbon absorbed in the North Sea has the potential for long term sequestration.

6.1 Experiment CO_2-NS

In experiment CO_2-NS we repeated the period 1980–2000 from experiment CWE (Table 1) but fixed the atmospheric pCO_2 to 1112 ppm over the North Sea whereas for the rest of the ocean the atmospheric pCO_2 is as in experiment CWE (Table 1). As expected, experiment CO_2-NS is marked by immediately high carbon fluxes into the North Sea in response to the sudden increase of atmospheric pCO_2. After the initial

BGD
9, 16625–16662, 2012

NW European shelf under climate warming

M. Gröger et al.

adaptation period of about 2 months only those areas are marked by strong carbon absorption where low pCO_2 waters from outside enter the North Sea (Fig. 7a) like in the English channel and east of Scotland. Waters leaving the North Sea via the Norwegian coastal current are marked by vigorous degassing. Along the pathway of North Sea water a plume of pronounced DIC enrichment is visible (Fig. 7b). Most of this water enters the Barents Sea via the Norwegian Current at a core depth of around 100 m. There is no significant portion that reaches directly the deep convection sites in the Greenland Sea.

Already after 20 yr of integration the air-sea carbon fluxes are in equilibrium and show no significant trend in experiment CO_2-NS. In experiment CO_2-NS the North Sea still absorbs 6.03 Mt C month^{-1} more compared to experiment CWE. If all of the carbon absorbed over the North Sea would be sequestered in the deep open ocean, then the globally integrated oceanic carbon uptake should be enhanced by the same amount.

However, the global ocean uptake is rises by only 1.2 Mt C month^{-1} along the Norwegian Current (Fig. 7a). This means that only 19.9 % of the anthropogenic carbon absorbed in the North Sea has the potential for longer term sequestration in the open ocean. The first order effect of higher absorption over the North Sea is thus enhanced degassing in the open Atlantic. The efficiency of shelf carbon pumping is thus very low. Moreover, we repeated this experiment but simulated the period 2080–2100 instead of 1980–2000 to find out whether or not the carbon shelf pumping is also very vulnerable to the climate warming in the course of the 21st century. From this experiment we calculate that at the end of the 21st century only 13.6 % of carbon absorbed over the North Sea is being stored for longer in the open ocean. This means that the efficiency of carbon shelf pumping is also highly vulnerable to climate warming.

6.2 Experiment MARKER

In order to explain the mechanism behind the low efficiency of the carbon shelf pump, we carried out experiment MARKER (Table 1). This experiment was designed to

BGD
9, 16625–16662, 2012

NW European shelf under climate warming

M. Gröger et al.

quantify the amount of North Sea water that reaches the open ocean without undergoing intense modification by air sea gas exchange.

In ensemble experiment MARKER 10 model runs were restarted from experiment CWE at the first of July in subsequent years from 1975 to 1984. In these experiments the North Sea water was initialized with a tracer concentration of 1 whereas outside the North Sea the tracer was initialized with a concentration of 0. The tracer concentration in subsurface layers was subject to advection and diffusion only. In the model's surface layer the tracer concentration was additionally altered by a simple air-sea gas exchange using a fixed air tracer concentration of 0 and a characteristic piston velocity of 100 $m\,yr^{-1}$. The tracer inventory found outside the North Sea is thus an approximate measure for the potential of the North Sea shelf to really enrich the ocean with the tracer. We chose the 1 July for starting the ensemble members because at this time the water column in the North Sea is strongly stratified. Thus, tracer rich bottom waters are sheltered from exposure to the atmosphere and have highest potential to reach the open ocean.

The results of experiments MARKER show that already within the first year the marked North Sea water stock is reduced to less than 15 % of the initial volume 37 494 km^3 (Fig. 8, red line). After this steep decline the marked North Sea water stock is further reduced at low rates between 2 and 3 $km^3\,day^{-1}$. With the beginning of the next cold season (after around 500 days of integration) the mixed layer thickens again which results in slightly enhanced decomposition rates in the range of 10 to 15 $km^3\,day^{-1}$. After four years a stock of only 955 km^3 (2.6 % of the initial stock) exists which is decomposed at rates between 0.2 km^3 in summer and 0.7 $km^3\,day^{-1}$ in winter. About 98 % of this stock is located outside the North Sea in the open ocean (Fig. 8c, blue line). However, at the end of experiment MARKER only 188 km^3 are stored at depths below 1000 m (Fig. 8, green line) though this stock still is slightly growing at a rates of approximately 0.1 $km^3\,yr^{-1}$. In conclusion, the rapid decomposition of the North Sea stock as well as the very low amount of North Sea water stored at depths

Discussion Paper | Discussion Paper | Discussion Paper | Discussion Paper |
BGD
9, 16625–16662, 2012
NW European shelf under climate warming
M. Gröger et al.

below 1000 m clearly indicates that most of the water exported from the North sea remains in the ocean's mixed layer where it is still exposed to the atmosphere.

7 Potential implications for industrial fishery

Today, the North Sea is intensively exploited by industrial fishery which catches about 2 million tons fish per year (FAO, 2003). The modelled warming of the North Sea in combination with the predicted strong decline in primary production may negatively influence the entire food chain up to higher trophic fish. There is strong evidence that rising temperatures will lower growth rates and reproductivity of, e.g. Atlantic cod in the North Sea by increasing the metabolic stress (Millner et al., 2001; Pörtner et al., 2001; Pörtner and Farrel, 2008).

The effect of declining primary production on fisheries is less clear. On the one hand Pauly et al. (2002) indicated that on shelfs only about 35 % of the primary production is required to sustain today's fish catches. On the other hand there is growing evidence that primary production constraints fishery at least on large scale marine ecosystems (Chassot et al., 2010). In recent comprehensive observations the average chlorophyll concentration has been found to be a much better predictor for fishery than primary productivity. Friedland et al. (2012) found a strong positive relationship between the chlorophyll concentration and fishery catches in 52 large scale marine ecosystems. The decline of productivity in experiment CWE-CEE-AES is paralleled by a decrease of the yearly average phytoplankton and chlorophyll concentration by 25 %. However, our model neglects possible ecological responses of the phytoplanktonic ecosystem to changing nutrient inventories such as changes in the average size of phytoplankton, changes in the pathway of energy transfer (i.e. the number of trophic links between phytoplankton and fish), changes in the ingestions rates of mesoscale zooplankton (Friedland et al., 2012), as well as size dependent sinking speeds and thus, the ratio of particle export to primary production. Thus, the lack of more realistic ecosystem dynamics imposes some uncertainty on our assertions on future fisheries. On the other

BGD
9, 16625–16662, 2012

hands it appears hard to imagine that a drop of up to 50 % of nutrient imports from the Atlantic would remain without any consequences for fish stocks in the North Sea. We therefore suppose that in the warmer climate at the end of 21st century the weakening primary productivity will put forward stress on fishes of higher trophic levels and threaten economic fisheries in the North Sea in addition to direct temperature stress.

8 Summary and conlusions

Most global models (Steinacher et al., 2010) predict a decrease between 2 % and 20 % in open ocean productivity in response to climate warming. We have shown that on the NW European shelf the reduction in productivity is much stronger due to the suppression of lateral nutrient input resulting from the weakening of vertical mixing along the shelf break. This process is essential for both, the nutrient supply to the outer shelf and productivity and can be considered as most vulnerable under climate warming. In case of the North Sea the nutrient transport from the deep Atlantic declines by up to ~ 50 % in the 21st century and productivity decreases by ~ 35 % assuming current rates of anthropogenic nutrient eutrophication. Even if we neglect anthropogenic eutrophication in our simulations (experiments CWE and CEE) the shelf productivity is reduced by about ~ 30 % in the North Sea and on the entire NW European shelf (Table 4). This is twice as strong as the reduction in open ocean productivity.

Due to the declining biological production during the 21st century, the absorption of carbon dioxide in the North Sea (on the NW European shelf) likewise reduces by 34 % (21 %) or 37 % (32 %) when anthropogenic eutrophication is considered in the simulations.

This study supports observational evidence that the NW European shelf is an active sink for atmospheric CO_2 (e.g. Frankignoulle and Borges, 2001). However, our results do not support the hypothesis that this leads to a substantially enhanced open ocean storage due to shelf sea pumping as proposed by Thomas et al. (2004). Water tracer experiments clearly indicate that most of the carbon dioxide absorbed on the shelf is

BGD
9, 16625–16662, 2012

not removed permantantly from the atmosphere because most of the shelf water does not reach the deep ocean but remains within the ocean's mixed layer where it is still exposed to the air sea gas exchange. We estimate that only ∼20 % of the carbon absorbed in the North Sea contributes to the long term oceanic carbon uptake. This fraction will be further reduced as a consequence of anthropogenic climate change.

Appendix A

Light extinction scheme

A pronounced feature of the North Sea is the strong seasonal cycle of nutrient concentration and primary production. During winter photosynthesis and phytoplankton growth is strongly limited by light resulting in lower productivity and higher nutrient concentrations compared to summer when primary production is limited by nutrients due to strong stratification. In spring increasing short wave radiation stimulates the characteristic spring phytoplankton bloom in the North Sea (e.g. Moll, 1998). Light intensity in the water column is further reduced due to absorption and scattering. Hence, for a realistic simulation of the timing and intensity of the spring bloom, a proper and physically consistent formulation of light penetration into the water column is necessary.

We therefore had to adopt a more elaborated scheme for light penetration that considers the variation of light intensity within individual grid cells. In Maier-Reimer et al. (2005) it was assumed that the light reaching the top of a box be effective over the whole box. For the open ocean this turned out to be a tolerable approximation. For our present model configuration with large regions of shallow water and the increased thickness of the surface layer it turned out to be no longer acceptable. As the mixing transport of light aborbing particles to depth is blocked by the bottom, it favoured a substantial bloom in the Southern North Sea already in February.

Light intensity is calculated from downward shortwave radiation at the surface $I(0)$ which is attenuated with depth Z by applying the attenuation coefficient atten in the

BGD
9, 16625–16662, 2012

following form:

$$I(Z) = I(0) \times \exp(-\text{atten} \times Z) \tag{A1}$$

Because atten is variable to changing concentrations of chlorophyll in space and time, in the standard version of HAMOCC (Eq. A1) is discretized onto the vertical $z(k)$ layers as

$$I(k) = I(k-1) \times \exp(-\text{atten} \times dz(k-1)) \tag{A2}$$

Hence, the light intensity at the top of the water column $I(0)$ is assumed for the entire layer thickness $z(1)$. Over the first 16 m of the surface layer no light attenuation is assumed. For clear waters in the open ocean this assumption has been proven to well reproduce global fields of nutrients and primary production. Under the turbid conditions on shallow shelfs and near the coasts where high loads of suspended matter from rivers can reduce the most of radiation already after a few meters this assumption is no longer realistic. As a consequence, the standard model simulates a first phytoplankton bloom already in early February in the Southern North Sea (Fig. 9b) which is contrary to and other studies (e.g. Moll, 1998; Paetsch and Kühn, 2008; Prowe et al., 2009).

For the present study we calculated an effective light intensity for all euphotic layers by integrating (Eq. A1) in the following way:

$$I_{\text{eff}}(k) = \frac{I(k-1)}{\text{atten} \times dz(k)} \times (1 - \exp(-\text{atten} \times dz(k))) \tag{A3}$$

The second change we implemented refers to the fact that near the coasts light is attenuated additionally by resuspended silt due to vigorous tidal currents (Heath et al., 2002; Paetsch and Kühn, 2008). The process of resuspension follows the empirical approach for the North Sea of Dobrynin (2009). The photosynthetic active radiation (PAR, Fig. 9) is then calculated as the sum of red and blue fractions and by expanding

BGD
9, 16625–16662, 2012

atten for the blue fraction according to

$$\mathrm{PAR}(z) = \mathrm{PAR}(0)\Big(\overbrace{R\exp(-zk_\mathrm{r})}^{\text{red fraction}} + \overbrace{(1-R)\exp\Big(-zk_\mathrm{w} - k_\mathrm{chl}\int_0^z \mathrm{chl}(z')\mathrm{d}z' - k_\mathrm{s}\int_0^z s(z')\mathrm{d}z'\Big)}^{\text{blue fraction}}\Big) \tag{A4}$$

with the attenuation coefficients for sea water scattering $k_\mathrm{w} = 0.03\,\mathrm{m}^{-1}$, chlorophyll α $k_\mathrm{chl} = 0.04\,(24.4\,\mathrm{g\,Chl\,m}^{-3})^{-1}\,\mathrm{m}^{-1}$ (where we adopted a relationship 60 between phytoplankton bound carbon and chlorophyll), and silt $k_\mathrm{s} = 0.06\,(\mathrm{g\,m}^{-3})^{-1}\,\mathrm{m}^{-1}$. The strongly attenuating red fraction $R = 0.4$ is calculated using $k_\mathrm{r} = 0.35\,\mathrm{m}^{-1}$.

The representation of the characteristic spring phytoplankton bloom substantially benefits from the improved light scheme (Fig. 9a, c). The unrealistically high light intensity of the standard light scheme forces a first phytoplankton bloom already in February (Fig. 9b). This is in strong contrast to observations which indicate that the main spring bloom occurs not before April (e.g. Moll, 1998). While the total productivity is nearly unchanged when using the improved light scheme instead of the standard scheme, the seasonal cycle is substantially improved.

Acknowledgements. We thank Katharina Six for intense revision of the manuscript which resulted in a significant improvement of the manuscript. Johannes Paetsch, Institute for Oceanography, University of Hamburg, provided daily loads of river nutrients between 1976 and 2006. This study was supported by the Federal Ministry of Education and Research, Germany, research grant 03F0443E AP3.1 (BMBF Nordatlantikprojekt II). Inga Hense, Institute of Hydrobiology and Fishery Science, University Hamburg helped in arguing about consequences on fishery.

The service charges for this open access publication
have been covered by the Max Planck Society.

References

Beaugrand, G.: The North Sea regime shift: evidence, causes, mechanisms and consequences, Prog. Oceanogr., 60, 245–262, 2004.

Bergeron, J.-P. and Koueta, N.: Biological productivity enhancement over a continental shelf break (Bay of Biscay, NE Atlantic) evidenced by mesozooplankton aspartate transcarbamylase activity, J. Oceanogr., 67, 249–252, 2011.

Chassot, E., Bonhommeau, S., Dulvy, N. K., Melin, F., Watson, R., Gascuel, D., and Le Pape, O.: Global marine primary production constrains fisheries catches, Ecol. Lett., 13, 495–505, doi:10.1111/j.1461-0248.2010.01443.x, 2010.

Chen, C.-T. A. and Borges, A. V.: Reconciling opposing views on carbon cycling in the coastal ocean: continental shelves as sinks and near-shore ecosystems as sources of atmospheric CO_2, Deep-Sea Res. Pt. II, 56, 578–590, 2009.

Dobrynin, M.: Investigating the Dynamics of Suspended Particulate Matter in the North Sea Using a Hydrodynamic Transport Model and Satellite Data Assimilation, Reports of the GKSS Research Center, GKSS-Forschungszentrum Geesthacht GmbH, 12/2009, 93 pp., ISSN 0344-9629, 2009.

Food and Agriculture Organization of the United Nations: The State of World Fisheries and Aquaculture, Rome, ISSN 1020-5489, available at: http://www.fao.org/docrep/013/i1820e/i1820e.pdf, 2010.

Frankignoulle, M. and Borges, A.: European continental shelf a significant sink for atmospheric carbon dioxide, Global Biogeochem. Cy., 15, 560–576, 2001.

Friedland, K. D., Stock, C., Drinkwater, K. F., Link, J. S., Leaf, R. T., Shank, B. V., Rose, J. M., Pilskaln, C. H., Michael J., and Fogarty, M. J.: Pathways between primary production and fisheries yields of large marine ecosystems, PLoS ONE 7, e28945, doi:10.1371/journal.pone.0028945, 2012.

Garcia, H. E., Locarnini, R. A., Boyer, T. P., Antonov, J. I., Zweng, M. M., Baranova, O. K., and Johnson, D. R.: World Ocean Atlas 2009, vol. 4, Nutrients (phosphate, nitrate, silicate), edited by: Levitus, S., NOAA Atlas NESDIS 71, US Government Printing Office, Washington, DC, 398 pp., 2010.

Gröger, M. and Mikolajewicz, U.: Note on the CO_2 air-sea gas exchange at high temperatures, Ocean Model., 39, 284–290, doi:10.1016/j.ocemod.2011.05.003, 2011.

Grosse, F. and Moll, A.: Validation Tool for Analyzing Vertical Profile Data of One State Variable (valpro1var) by Comparison of Merged Observational Data Sets and Their Preparation (OBS_prep) – Description and User Guide, Technical Reports 01-2011, Institute of Oceanography, Hamburg, Germany, 2011.

Heath, M. R., Edwards, A. C., Paetsch, J., and Turell, W. R.: Modelling the behaviour of nutrients in the coastal waters of Scotland, Fisheries Research Services Marine Laboratory Aberdeen, Scottish Executive Central Research Unit Contract, 106 pp., 2002.

Kühn, W., Paetsch, J., Thomas, H., Borges, A. V., Schiettecatte, L. S., Bozec, Y., and Prowe, A. E. F.: Nitrogen and carbon cycling in the North Sea and exchange with the North Atlantic – a model case study, Part II: Carbon budget and fluxes, Cont. Shelf Res., 16, 1701–1716, 2010.

Lorkowski, I., Pätsch, J., Moll, A., and Kühn, W.: Interannual variability of carbon fluxes in the North Sea from 1970 to 2006 – Comparing effects of abiotic and biotic drivers of the gas-exchange of CO_2, Esutar. Coast. Shelf S., 100, 38–57, 2012.

Marsland, S. J., Haak, H., Jungclaus, J. H., Latif, M., and Röske, F.: The Max Planck Institute global ocean/sea-ice model with orthogonal curvilinear coordinates, pelagic production at the Celtic Sea shelf break (1995), Ocean Model., 5, 91–127, 2003.

Maier-Reimer, E., Kriest, I., Segschneider, J., and Wetzel, P.: The Hamburg Ocean Carbon Cycle Model HAMOCC 5.1 – technical description release 1.1, Reports on Earth System Science, 14, 50 pp., available at: http://www.mpimet.mpg.de/fileadmin/publikationen/erdsystem_14.pdf, 2005.

Millner, R. S., Pilling, G. M., McCully, S. R., and Høie, H.: Changes in the timing of otolith zone formation in North Sea cod from otolith records: an early indicator of climate-induced temperature stress, Mar. Biol., 158, 21–30, doi:10.1007/s00227-010-1539-9, 2011.

Moll, A.: Regional distribution of primary production in the North Sea simulated by a three-dimensional model, J. Marine Syst., 16, 151–170, 1998.

Moll, A. and Radach, G.: Review of three-dimensional ecological modelling related to the North Sea shelf system, Part 1: Models and their results, Prog. Oceanogr., 57, 175–217, doi:10.1016/S0079-6611(03)00067-3, 2003.

Meybeck, M. and Ragu, A.: River Discharges to the Oceans: An Assessment of Suspended Solids, Major Ions and Nutrients, Unpublished report of the United Nations environmental Programme, 1995.

BGD
9, 16625–16662, 2012

New, A. L. and Pingree, R. D.: Evidence for internal tidal mixing near the shelf break in the Bay of Biscay, Deep-Sea Res., 37, 1783–1803, 1990.
Orr, J., Maier-Reimer, E., Mikolajewicz, U., Monfray, P., Sarmiento, J. L., Toggweiler, J. R., Taylor, N. K., Palmer, J., Gruber, N., Sabine, C.-L., Le Quere, C., Key, R. M., and Boutin, J.: Estimates of anthropogenic carbon uptake from four 3-D global ocean models, Global Biogeochem. Cy., 15, 43–60, 2001.
Paetsch, J. and Kühn, W.: Nitrogen and carbon cycling in the North Sea and exchange with the North Atlantic – a model study. Part I. Nitrogen budget and fluxes, Cont. Shelf Res., 28, 767–787, 2008.
Paetsch, J. and Lenhart, H.-J.: Daily loads of nutrients, total alkalinity, dissolved inorganic Carbon and dissolved organic Carbon of the European continental rivers for the years 1977–2002, Reports Center for Marine und Climate Research – Series B: Oceanography 2004, University of Hamburg, 2004.
Pauly, D., Christensen, V., Guenette, S., Pitcher, T. J., Rashid, T. U., Walters, C. J., Watson, R., and Zeller, D.: Towards sustainability in world fisheries, Nature, 418, 689–695, 2002.
Pingree, R. D. and Mardell, G. T.: Slope turbulence, internal waves, and phytoplankton groth at the Celtic Sea shelf break, Philos. T. R. Soc. Lond. A, 302, 663–682, 1981.
Pörtner, H. O. and Farrel, A. P.: Physiology and climate change, Science, 31, 690–692, 2008.
Pörtner, H. O., Berdal, B., Blust, R., Brix, O., Colosimo, A., De Wachter, B., Giuliani, A., Johansen, T., Fischer, T., Knust, R., Lannig, G., Naevdal, G., Nedenes, A., Nyhammer, G., Sartoris, F. J., Serendero, I., Sirabella, P., Thorkildsen, S., and Zakhartsevc, M.: Climate induced temperature effects on growth performance, fecundity and recruitment in marine fish: developing a hypothesis for cause and effect relationships in Atlantic cod (*Gadus morhua*) and common eelpout (*Zoarces viviparus*), Cont. Shelf Res., 21, 1975–1997, 2001.
Prowe, A. E. F., Thomas, H., Paetsch, J., Kühn, W., Bozec, Y., Schiettecatte, L.-S., Borges, A. V., and de Baar, H. J. W.: Mechanisms controlling the air-sea CO_2 flux in the North Sea, Cont. Shelf Res., 29, 1801–1808, 2009.
Raven, J. A. and Falkowski, P. G.: Oceanic sinks for atmospheric CO_2, Plant Cell Environ., 2, 741–755, doi:10.1046/j.1365-3040.1999.00419.x, 1999.
Roeckner, E., Lautenschlager, M., and Esch, M.: IPCC-AR4 MPI-ECHAM5_T63L31 MPI-OM_GR1.5L40, (pre-industrial control experiment): atmosphere 6 HOUR values MPImet/MaD Germany, World Data Center for Climate, Deutsches Klimarechenzentrum DKRZ GmbH, Hamburg, doi:10.1594/WDCC/EH5-T63L31_OM-GR1.5L40_CTL_6H, 2006.

BGD
9, 16625–16662, 2012

NW European shelf under climate warming

M. Gröger et al.

Steinacher, M., Joos, F., Frölicher, T. L., Bopp, L., Cadule, P., Cocco, V., Doney, S. C., Gehlen, M., Lindsay, K., Moore, J. K., Schneider, B., and Segschneider, J.: Projected 21st century decrease in marine productivity: a multi-model analysis, Biogeosciences, 7, 979–1005, doi:10.5194/bg-7-979-2010, 2010.
Sweby, P. K.: High resolution schemes using flux limiters for hyperbolic conservation laws, SIAM J. Numer. Anal., 21, 995–1011, 1984.
Taylor, K. E.: Summerizing multiple aspects of model performance in a single diagram, J. Geophys. Res., 106, 7183–7192, 2001.
Thomas, H., Bozec, Y., Elkalay, K., and de Baar, H. J. W.: Enhanced open ocean storage of CO_2 from shelf sea pumping, Science, 304, 1005–1008, 2004.
Thomas, H., Bozec, Y., de Baar, H. J. W., Elkalay, K., Frankignoulle, M., Schiettecatte, L.-S., Kattner, G., and Borges, A. V.: The carbon budget of the North Sea, Biogeosciences, 2, 87–96, doi:10.5194/bg-2-87-2005, 2005.
Thomas, M., Sündermann, J., and Maier-Reimer, E.: Consideration of ocean tides in an OGCM and impacts on subseasonal to decadal polar motion excitation, Geophys. Res. Lett., 28, 2457–2460, 2001.
Tsunogai, S., Watanabe, S., and Sato, T.: Is there a continental shelf pump for the absorption of atmospheric CO_2?, Tellus B, 51, 701–712, 1999.
Uriarte, A. and Lucio, P.: Migration of adult mackerel along the Atlantic European shelf edge from a tagging experiment in the south of the Bay of Biscay in 1994, Fish Res., 50, 129–139, 2001.
Wetzel, P., Winguth, A., and Maier-Reimer, E.: Sea to air CO_2 flux from 1948 to 2003, a model study, Global Biogeochem. Cy., 19, GB2005, doi:10.1029/2004GB002339, 2005.
Wanninkhof, R.: Relationship between wind speed and gas exchange over the ocean, J. Geophys. Res., 97, 7373–7382, 1992.
Wollast, R.: Continental margin – review of geoachemical settings, in: Ocean Margin Systems, edited by: Wefer, G., Billet, D., Hebbeln, D., Joergenson, B. B., Schlueter, M., and van Weering, T. C. E., Springer Verlag, Berlin Heidelberg New York, 15–31, 1998.

BGD
9, 16625–16662, 2012

NW European shelf under climate warming

M. Gröger et al.

Table 1. Model experiments. CWE = climate warming effect, CEE = carbon emission effect, AES = anthropogenic eutrophication scenario.

Experiment	pCO_2	Eutroph.	Period
CTRL	288	no	without climate warming 1860–2100
CWE	288	no	1860–2100
CWE-CEE	288–700 ppm	no	1860–2100
CWE-CEE-AES	288–700 ppm	yes	1860–2100
CO_2-NS	288 ppm but NS: 1112 ppm	no	1980–2000
MARKER	288 ppm	no	10 runs of 5-yr integration[1]

[1] Ensemble runs were start on 1 July 1975, 1 July 1976, 1 July 1979.

BGD
9, 16625–16662, 2012

NW European shelf under climate warming

M. Gröger et al.

Table 2. Modeled global and regional mass fluxes averaged for the last decade of the 20th century. Mass fluxes for the North Sea refer to Thomas et al. (2005). NB = northern boundary, EC = English Channel, ATM = atmpshere, P–E = Precipitation–Evaporation.

Global	other Models	Model
Primary Production ($Pg\,C\,yr^{-1}$)	24–49[1]	54
Export Production ($Pg\,C\,yr^{-1}$)	5.0–9.9[1]	7.2
Carbon uptake 1990–1999 ($Pg\,C\,yr^{-1}$)	1.5–2.2[2]	1.55
North Sea	Observation	Model
$Volume_{NB}$ (Sv)	−0.18	−0.19 (±0.05)
$Volume_{EC}$ (Sv)	0.15	0.17 (±0.04)
P-E (Sv)		−0.02 (±0.004)
$Carbon_{NB}$ ($Tmol\,yr^{-1}$)	−13.3	−9.9 (±3.1)
$Carbon_{EC}$ ($Tmol\,yr^{-1}$)	10.7	9.0 (±3.9)
$Carbon_{ATM}$ ($Tmol\,yr^{-1}$)	0.8	0.9 (±0.008)

[1] Steinacher et al. (2010).
[2] Orr et al. (2001).

BGD
9, 16625–16662, 2012

Table 3. Statistics for a quantitative comparison of simulated and observed state variables derived from Taylor diagrams (Taylor, 2001). rms = root mean squared, corr = Pearson's correlation, stddev = standard deviation.

State variable	rms	corr	stddev observation	stddev simulation
Phosphate	0.25	0.58	0.29	0.24
Nitrate	6.10	0.43	6.00	5.50
Temperaturte	1.20	0.94	3.40	2.90
Salinity	0.75	0.76	1.10	1.10

BGD
9, 16625–16662, 2012

Table 4. Budgets of absorption (defined as net C-flux into the water column in Mio. tons of carbon) and biological production (Mio. tons of carbon) for the North Sea calculated over the last two decades of the 20th and 21st centuries. Numbers in brackets indicate budgets calculated for the entire NW European shelf (= all areas 37° N and 65° N adjacent to the North Atlantic and shallower than 200 m). Last two columns indicate the relative change from 1980–1999 to 2080–2099. PP = Primary productivity.

Experiment	1980–1999		2080–2099		relative change (%)	
	PP	Absorption	PP	Absorption	PP	Absorption
CWE	31.07	9.3	21.68	7.15	−30.22	−23.11
	(84.74)	(18.29)	(60.81)	(16.05)	(−28.24)	(−12.25)
CWE-CEE	31.66	9.89	21.66	6.53	−31.58	−33.97
	(85.76)	(21.16)	(60.02)	(16.61)	(−30.01)	(−21.50)
CWE-CEE-AES	40.04	11.80	25.82	7.43	−35.51	−37.03
	(130.29)	(29.52)	(79.04)	(20.03)	(−39.34)	(−32.15)

BGD
9, 16625–16662, 2012

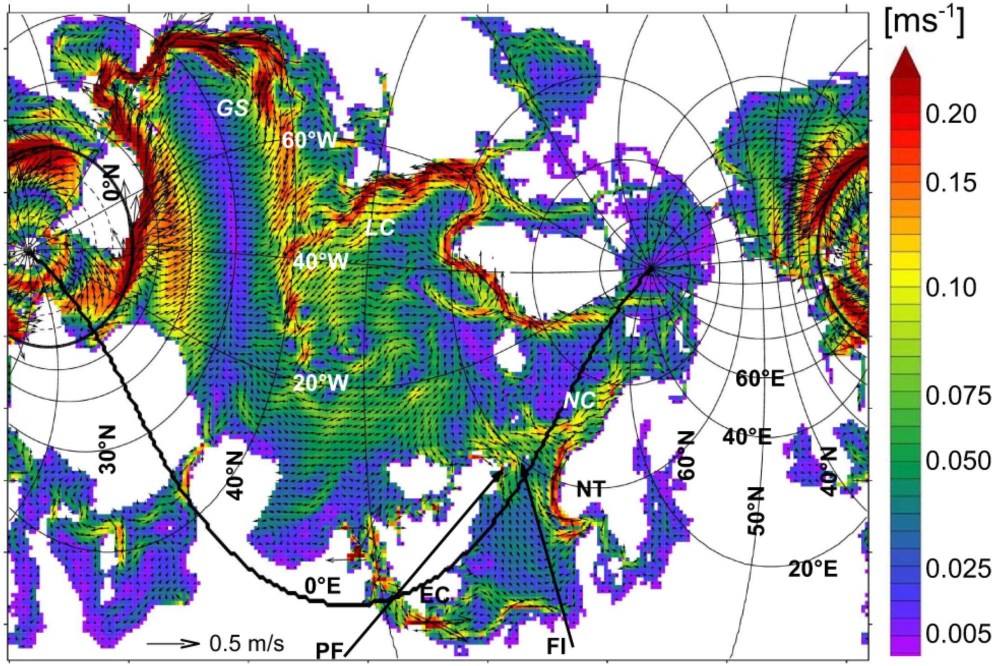

Fig. 1. Model domain. Also shown: surface circulation averaged over 1990–1999. Only every fourth vector is shown. EC = English Channel, NT = Norwegian Trench, PF = Pentland Firth, FI = Faire Island, NC Norwegian Current, LC = Labrador Current, GS = Gulf Stream.

BGD

9, 16625–16662, 2012

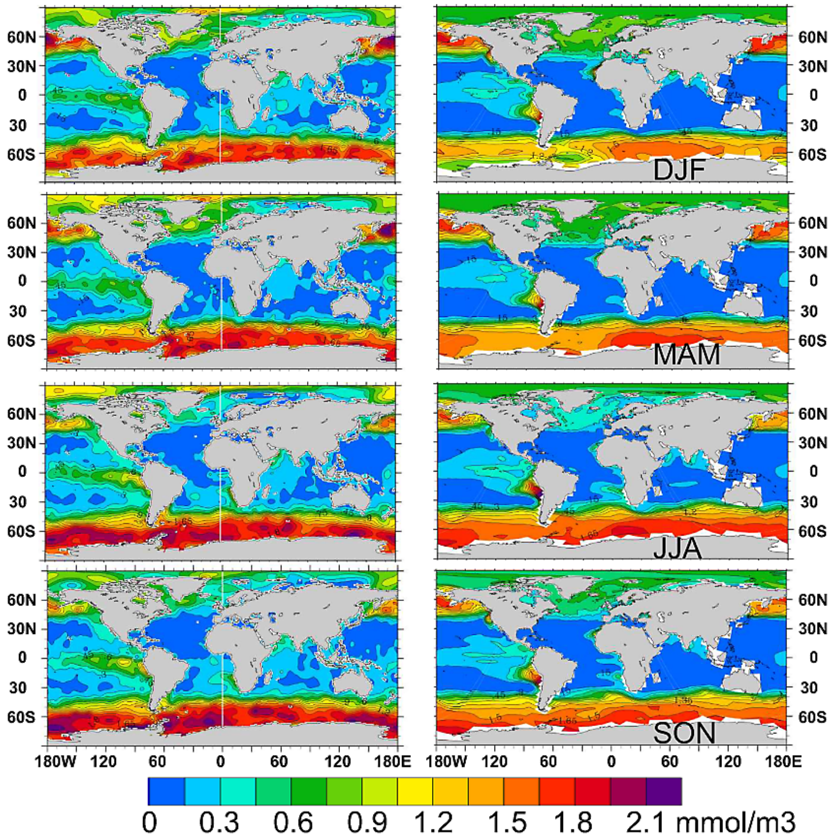

Fig. 2. Modelled seasonal cycle of surface phosphate (right hand) compared to observations from the World Ocean Atlas (left hand, Garcia et al., 2010).

BGD

9, 16625–16662, 2012

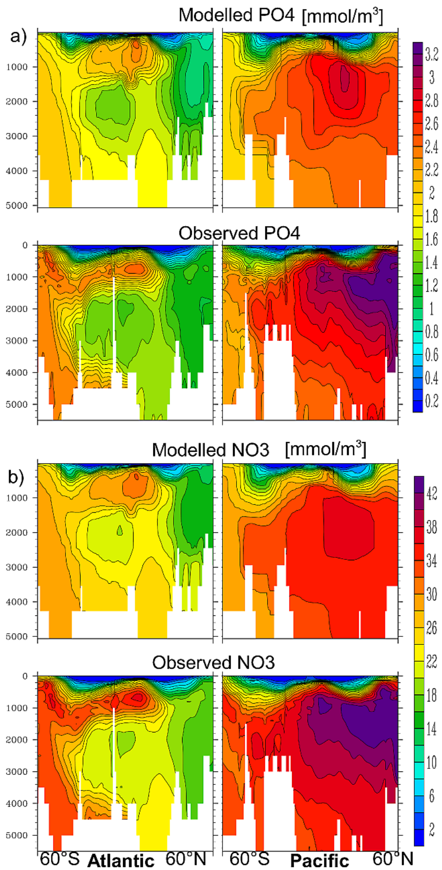

Fig. 3. Modelled annual mean distributions for phosphate **(a)** and nitrate **(b)** along 35° W (Atlantic, left) and 180° E (Pacific, right) compared to observations from the World Ocean Atlas (Garcia et al., 2010).

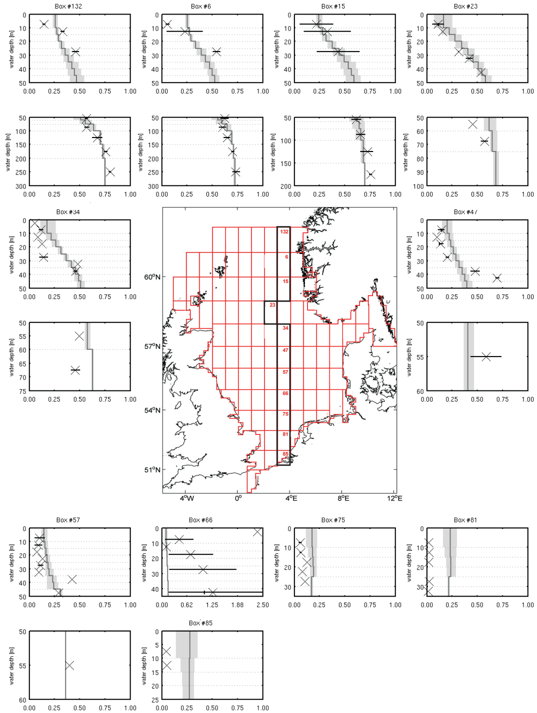

Fig. 4. North–south transect of phosphate profiles through the North Sea as climatological monthly means for May (1993–2006) for observation (crosses with minimum and maximum bars) and simulation (mean profile solid line and variability (17 % and 83 % percentile) as shading). The profiles begin with the most northern box in the top left corner and ending in the most right subplot at the bottom. The selected boxes are marked in the box configuration. Vertical profiles with data observed deeper than 50 m are separated into two plots for a better resolution. The lower part of the profile is always positioned directly below the according upper part.

BGD
9, 16625–16662, 2012
NW European shelf under climate warming
M. Gröger et al.

Title Page
Abstract Introduction
Conclusions References
Tables Figures
◀ ▶
Back Close
Full Screen / Esc
Printer-friendly Version
Interactive Discussion

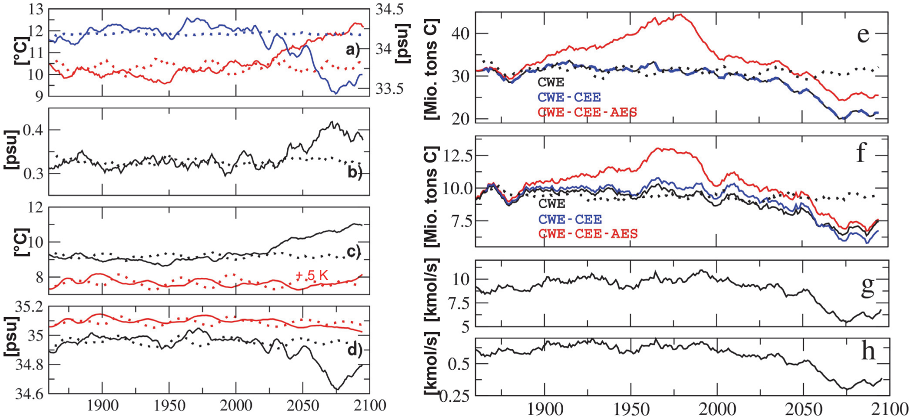

Fig. 5. (a) annual mean of surface temperature (red) and salinity (blue) averaged over the North Sea. Dotted lines indicate the control integration CTRL, **(b)** annual mean bottom-surface salinity difference averaged over the North Sea, **(c)** 0–100 m (black) and 614–713 m (red) water temperature averaged over the continental slope north of the North Sea (2° W–10° N; 60°–65° N), the red curve has been shifted by +5 K along the y-achsis to facilitate comparison with black curve. **(d)** same as **(c)** but for salinity, **(e)** yearly primary production integrated over the North Sea. Dotted lines indicate the control integration CTRL, **(f)** Carbon absorption of the North Sea (Mt C). Dotted lines indicate the control integration CTRL, **(g)** winter gross mass transports of nitrate into the North Sea calculated from experiment CWE, **(h)** same as **(g)** but for phosphate. Note: Hydrographic properties in **(a–d)** are the same in all experiments.

BGD
9, 16625–16662, 2012

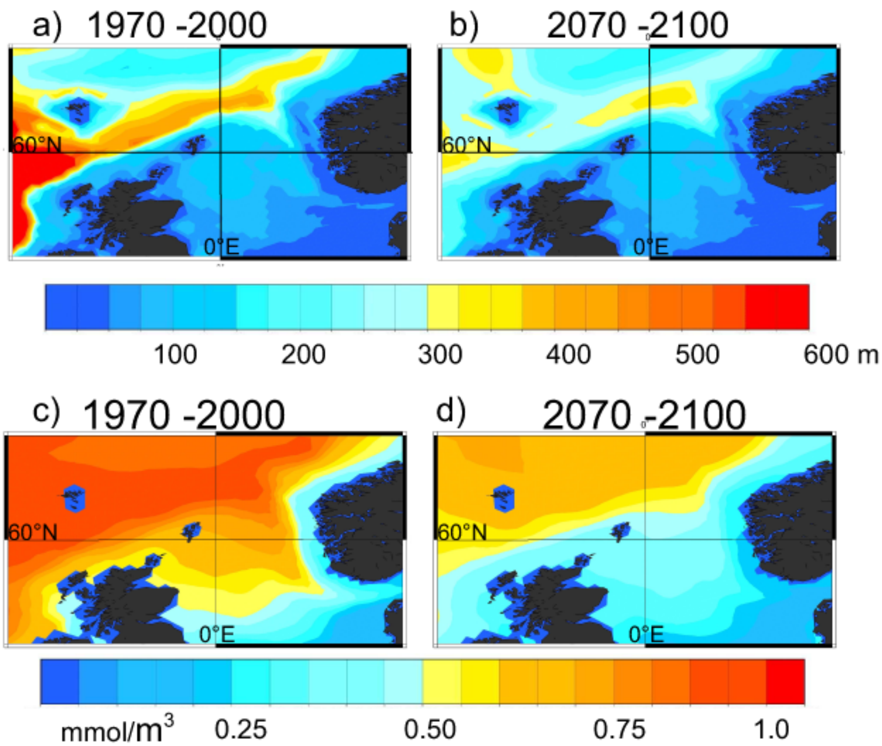

Fig. 6. (a) and **(b)**: Average Winter (DJF) mixed layer depth at the end of the 20th and 21st Century. **(c)** and **(d)**: Same as **(a)** and **(b)** but for average dissolved surface phosphate concentration.

BGD
9, 16625–16662, 2012

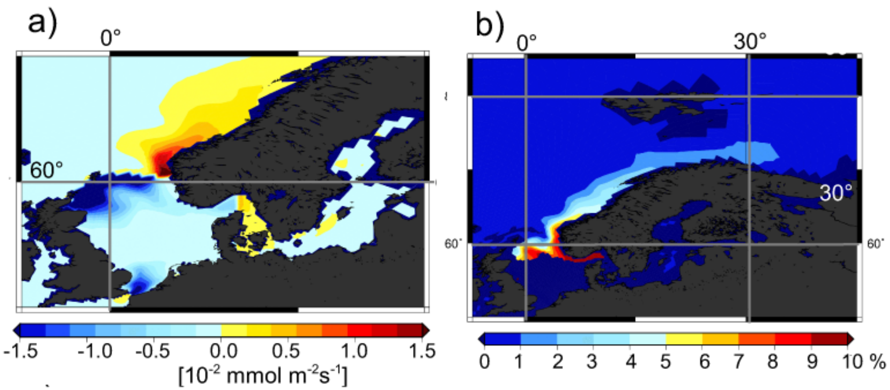

Fig. 7. (a) Sea–air carbon flux in experiment CO_2-NS. An 10 yr average of 1990–1999 is shown. Positive flux indicates degassing. **(b)** Relative change of dissolved inorganic carbon at 95 m depth between experiments CO_2-NS minus experiment CWE. Positive values indicate higher concentrations in exeriment CO_2-NS. An average over the years 1995–1999 is shown.

BGD

9, 16625–16662, 2012

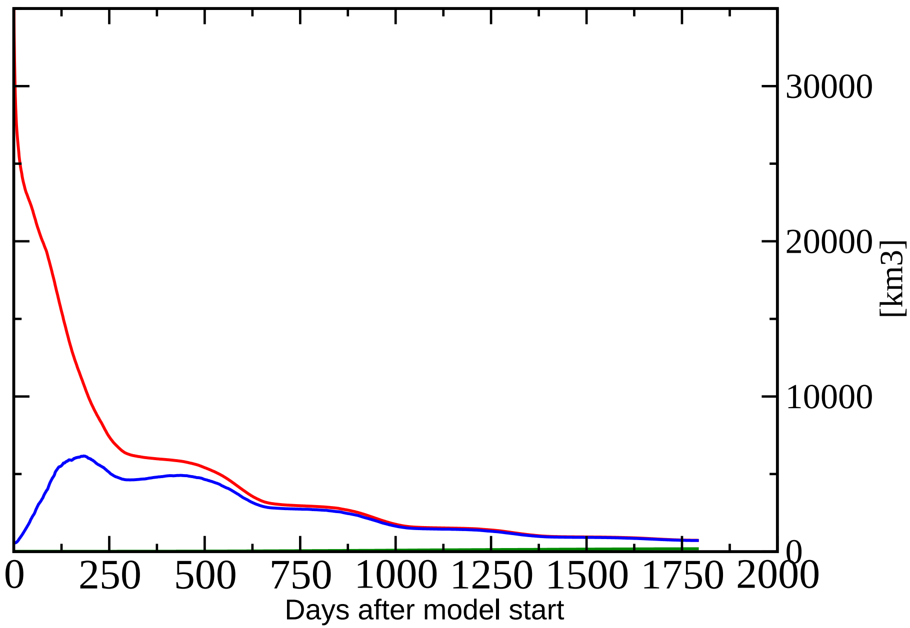

Fig. 8. Inventory of marked North Sea water in experiment MARKER. An average over all ensemble members is shown. Red line indicates the total ocean inventory. Blue line indicates open ocean inventory without the North Sea and green line indicates the deep ocean inventory below 1000 m water depth. The inter-ensemble variability is very low compared to mean signal.

BGD
9, 16625–16662, 2012

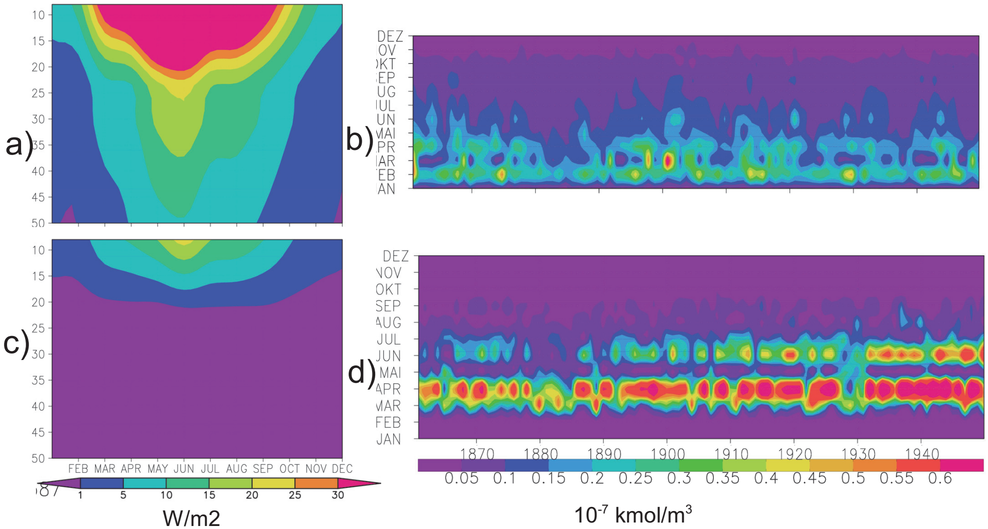

Fig. 9. **(a)** Available photosynthetic active short wave radiation averaged over the North Sea south of 54° N using standard light scheme. **(b)** Seasonal cycles of phytoplankton (in *P* units) concentration using standard light scheme. **(c)** and **(d)** Same as **(a)** and **(b)** but using modifyed light scheme.

BGD
9, 16625–16662, 2012